Spectroscopic Studies of Protonated Aromatic Species and Radical Cations in H^+-Zeolites

Xinsheng Liu,[†] Kai-Kong Iu,[†] J. Kerry Thomas,*[,†] Heyong He,[‡] and Jacek Klinowski[‡]

Contribution from the Department of Chemistry and Biochemistry, University of Notre Dame, Notre Dame, Indiana 46556, and Department of Chemistry, University of Cambridge, Lensfield Road, Cambridge CB2 1EW, U.K.

Received May 23, 1994[⊗]

Abstract: The formation of cation radicals and protonated species of *all-trans*-1,6,-diphenylhexatriene, anthracene, pyrene, and perylene in zeolites H^+-ZSM-5, H^+-mordenite, and H^+-Y was studied using solid-state NMR and diffuse reflectance and fluorescence spectroscopies. The two types of species form concurrently, and cation radicals are more stable than the corresponding protonated species. The Brønsted acid sites are responsible for the formation of the protonated species, and the Lewis acid sites, associated nonframework Al atoms, for the formation of cation radicals. In contrast to solutions of strong acids, the transformation of protonated species into cation radicals does not occur in zeolites, where they revert to the original neutral molecules instead. Exposure of the samples to laboratory air accelerates this process, and only cation radicals are observed afterward. The stabilities of cation radicals and protonated species depend on the size of zeolitic cavities and channels and on the nature of the aromatic molecules. Further reactions of cation radicals are observed in zeolites with large interstitial space.

Introduction

H^+-forms of zeolites contain the Brønsted and Lewis acid sites[1] and are important acidic catalysts used in a number of processes, particularly in the petrochemical industry. The understanding of the nature of the acid sites and their interactions with guest molecules is therefore essential. Brønsted acid sites in zeolites originate from the bridging ≡Si−OH−Al≡ groups, and their nature is well understood.[2] The nature of Lewis sites is more complex, and it has been suggested that a number of species, such as coordinatively unsaturated framework Al and Si atoms,[3,4] nonframework aluminum species,[4−7] and strained ≡Si−OH−Al≡ linkages,[8] are responsible. The formation of cation radicals, charge-transfer complexes, and ion pairs in zeolites under γ- and X-ray irradiation, photolysis with UV light, and other conditions is an active area of research.[9−12] One of the most significant outcomes of these studies is the recognition of the unique charge-stabilization properties of zeolites: cation radicals and ion pairs generated in the intracrystalline space could be very stable, in certain cases even permanent.[10] We present evidence for the *concurrent* formation of protonated species and cation radicals of *all-trans*-1,6-diphenylhexatriene (DPHT), anthracene (An), pyrene (Py), and perylene (Per) within the cavities and channels of zeolites H^+-ZSM-5, H^+-mordenite, and H^+-Y and discuss the nature of the Lewis acid sites responsible for the formation of cation radicals. Na^+-forms of the zeolites were investigated for comparison.

Experimental Section

Zeolites. Zeolites Na-Y (LZY-52, Si/Al = 2.5), NH_4-Y (LZY-82, Si/Al = 2.95), Na-mordenite (Na-M) (LZM-5, Si/Al = 5.3), and NH_4-mordenite (NH_4-M) (LZM-8, Si/Al = 9.0) were supplied by UOP and used as received. Na-ZSM-5 was synthesized without using an organic template[13] and TPA,Na-ZSM-5 using tetrapropylammonium chloride (TPACl).[14] X-ray diffraction (XRD) showed that Na-ZSM-5 with Si/Al = 15 and TPA,Na-ZSM-5 with Si/Al = 25 were pure and highly crystalline. The occluded template molecules were removed by calcination at 550 °C for 8 h. Calcined ZSM-5 was twice ion-exchanged with a 0.2 M aqueous solution of NaCl at room temperature to give the sample Na(ex)-ZSM-5. Zeolite H-Y was prepared by calcination of NH_4-Y (LZY-82) at 550 °C for 6 h. Ultrastable H-Y (UHY) was made by treatment of NH_4-Y under deep bed conditions at 550 °C for 18 h,[15] and zeolite H-M, by calcining NH_4-mordenite (LZM-8) at 550 °C for 6 h.

Loading of Organic Molecules. Zeolite samples were first activated at 500 °C in air for 5 h. A calcined sample (0.5−1 g) was then quickly dispersed in 5 mL of *n*-pentane immediately after being taken from the furnace. A 3×10^{-6} mol/mL solution (0.5-1 mL) of the probe molecule in *n*-pentane was then added, and the suspension was

[†] University of Notre Dame.
[‡] University of Cambridge.
[⊗] Abstract published in *Advance ACS Abstracts*, December 1, 1994.

(1) Turkevich, J.; Ciborowski, S. *J. Phys. Chem.* **1967,** *71,* 3208.
(2) Tanabe, K.; Misono, M.; Ono, Y.; Hattori, H. *New Solid Acids and Bases. Their Catalytic Properties;* Elsevier: Amsterdam, 1989; p 142.
(3) Stamires, D. N.; Turkevich, J. *J. Am. Chem. Soc.* **1964,** *86,* 749.
(4) Ward, J. W. In *Zeolite Chemistry and Catalysis;* Rabo, J. A., Ed.; ACS Monograph 171; American Chemical Society: Washington, DC, 1976; p 118.
(5) Ripmeester, J. A. *J. Am. Chem. Soc.* **1983,** *105,* 2925.
(6) Freude, D.; Hunger, M.; Pfeifer, H. *Z. Phys. Chem.* **1987,** *152,* 429.
(7) (a) Lunsford, J. H. *J. Phys. Chem.* **1968,** *72,* 4163. (b) Lunsford, J. H. *J. Catal.* **1969,** *14,* 379. (c) Lunsford, J. H.; Zingery, L. W.; Rosynek, M. P. *J. Catal.* **1975,** *38,* 179.
(8) Kutcherov, A. V.; Slinkin, A. A. In *Structure and Reactivity of Modified Zeolites;* Jacobs, P. A., Jaeger, N. I., Jírů, P., Kazansky, V. B., Schulz-Ekloff, G., Eds.; Elsevier: Amsterdam, 1984; p 77.
(9) (a) Qin, X.-Z.; Trifunac, A. D. *J. Phys. Chem.* **1990,** *94,* 4751. (b) Barnabas, M. V.; Trifunac, A. D. *Chem. Phys. Lett.* **1991,** *187,* 565. (c) Barnabas, M. V.; Trifunac, A. D. *Chem. Phys. Lett.* **1992,** *193,* 298.
(10) Ramamurthy, V.; Caspar, J. V.; Corbin, D. R. *J. Am. Chem. Soc.* **1991,** *113,* 594.
(11) (a) Iu, K.-K.; Thomas, J. K. *J. Phys. Chem.* **1991,** *95,* 506. (b) Iu, K.-K.; Thomas, J. K. *Colloids Surf.* **1992,** *63,* 39. (c) Iu, K.-K.; Liu, X.; Thomas, J. K. *J. Phys. Chem.* **1993,** *97,* 8165.
(12) (a) Yoon, K. B.; Kochi, J. K. *J. Phys. Chem.* **1991,** *95,* 1348. (b) Yoon, K. B.; Kochi, J. K. *J. Phys. Chem.* **1991,** *95,* 3780.
(13) Xiang, S.; Liu. S.; Wu, D.; Liu, Y.; Zhang, X.; Li, H. Faming Zhuanli Shenqing Gongkai Shuomingshu, CN85,100,463, 1986.
(14) Jacobs, P. A.; Martens, J. A. *Synthesis of High-Silica Aluminosilicate Zeolites;* Elsevier: Amsterdam, 1987; p 17.
(15) (a) McDaniel, C. V.; Maher, P. K. *Molecular Sieves;* Society of Chemical Industry: London, 1968; p 186. (b) McDaniel, C. V.; Maher, P. K. In *Zeolite Chemistry and Catalysis;* Rabo, J. A., Ed.; ACS Monograph 171; American Chemical Society: Washington, DC, 1976; p 285. (c) McDaniel, C. V.; Maher, P. K. U.S. Pat. 3,449,070, 1969.

0002-7863/94/1516-11811$04.50/0

Scheme 1. Schematic Drawing of (a) Probe Molecules and (b) Framework Structures of Zeolites ZSM-5, Mordenite, and Y

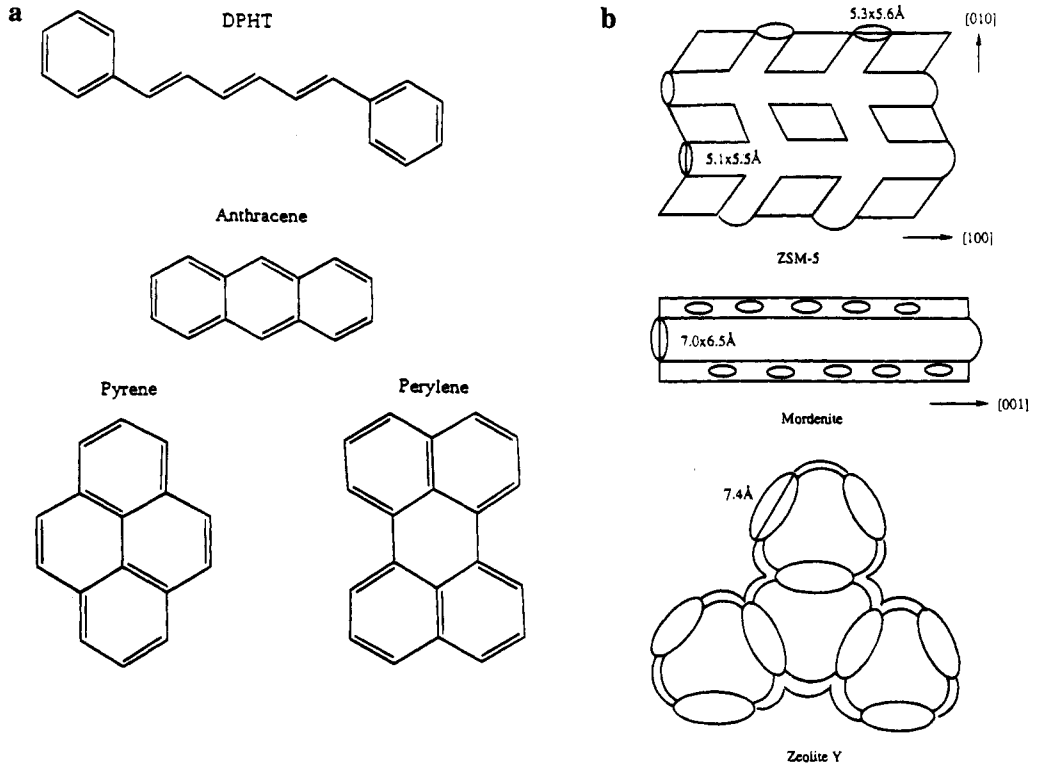

Table 1. Sizes of the Molecules and the Cavities and Channels of Zeolites

molecule	size (Å)
DPHT	5.58 × 16.34
An	5.59 × 9.79
Py	7.36 × 9.80
Per	7.33–7.37 × 9.82

zeolite	aperture size (Å)	dimensionality
ZSM-5	5.3 × 5.6 and 5.1 × 5.5	2
mordenite	7.0 × 6.5	1
Y	7.4	3

vigorously stirred. The solid was separated off by filtration and quickly transferred to a quartz cell cuvette, and the cuvette was evacuated. For the UV–vis diffuse reflectance experiments, the sample slurry was prepared directly in the spectrophotometer cell.

Instrumental Techniques. Magic-angle-spinning (MAS) NMR spectra were recorded at 9.4 T on a Chemagnetics CMX-400 spectrometer with 7.5 mm zirconia rotors spun in nitrogen at 4.5 kHz. ^{27}Al spectra were measured at 104.2 MHz with very short, 0.5 μs (less than 10°), radiofrequency pulses and 0.2 s recycle delays. ^{13}C CP/MAS NMR spectra were recorded at 100.6 MHz with 5 μs ^{1}H 90° pulses, 2 ms contact times, and 3 s recycle delays. Line positions for ^{27}Al and ^{13}C are given in ppm from external $Al(H_2O)_6^{3+}$ and TMS. UV–vis diffuse reflectance spectra were acquired using a Cary 3 spectrophotometer, and fluorescence spectra, with a SLM photofluorimeter. Lifetime measurements used dye lasers pumped with a 308 XeCl laser.

Results

We shall first consider the structures of the model compounds and the zeolites (see Scheme 1 and Table 1).[16] ZSM-5 has an orthorhombic structure with two intersecting channel systems composed of 10-membered rings of TO_4 tetrahedra (T = Si or Al). The dimensions of the zig-zag channels along the [010] direction are 5.3 × 5.6 Å and those of the straight channels along the [100] direction 5.1 × 5.5 Å. Mordenite is also orthorhombic, and the 12-membered ring channels along the [001] direction are wider (7.0 × 6.5 Å) than the 2.6 × 5.7 Å channels along the [010] direction. The latter channels are too small to accommodate our probe molecules. The structure of zeolite Y is cubic, and its three-dimensional pore system involves double-six-membered rings, sodalite cages (both with entry apertures of 2.6 Å), and tetrahedrally connected "supercages" with an entry aperture of 7.4 Å. Only the supercages are large enough to admit the guest molecules under study.

The sizes of the probe molecules given in Table 1 were calculated using a molecular modeling program.[17] The distance between the outermost hydrogens was measured after the molecules were energy-minimized. The molecular size was obtained by summing the H–H distance and twice the covalent radius of hydrogen (2 × 0.30 Å = 0.60 Å[18]). In perylene the distances between the two groups of outermost hydrogens are unequal, and both are given.

Structural Characterization

Calcination of NH_4^+-zeolites at 550 °C gives H^+-zeolites and causes partial dealumination of the framework. The expelled Al atoms migrate to the cavities and channels.[15,19,20] The degree of dealumination depends on the structure, the conditions of calcination, and the initial framework Si/Al ratio. The process has been extensively studied and is used for the ultrastabilization of zeolite Y, an important process for the preparation of cracking catalysts. The so-called "deep bed" and "shallow bed" condi-

(16) Meier, W. M.; Olson, D. H. *Atlas of Zeolite Structure Types*, 3rd ed.; Butterworths-Heinemann: London, 1992.

(17) Still, W. C.; Mohamad, F.; Richards, N. G.; Guida, W. C.; Lipton, M.; Liskamp, R.; Chang, G.; Hendrickson, T.; DeGunst, F.; Hasel, W. *MacroModel v2.5* Department of Chemistry, Columbia University, New York, NY 10027.

(18) Atkins, P. W. *Physical Chemistry*, 2nd ed.; W. H. Freeman: San Francisco, CA, 1982; p 756.

(19) Engelhardt, G.; Michel, D. *High-Resolution Solid State NMR of Silicates and Zeolites;* Wiley: New York, 1987; p 272.

(20) Klinowski, J. *Progr. NMR Spectrosc.* **1984**, *16*, 237.

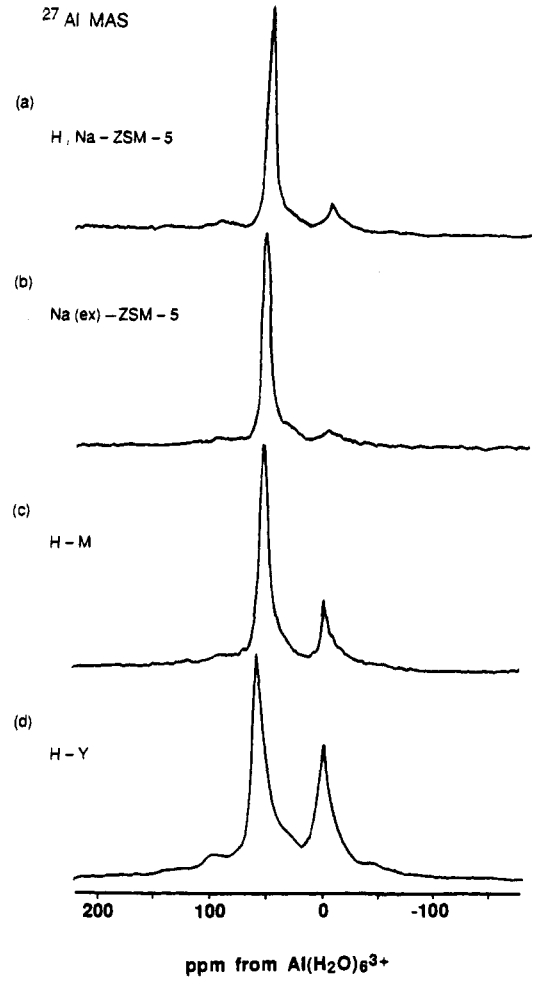

Figure 1. ^{27}Al MAS NMR spectra of (a) H,Na-ZSM-5, (b) Na(ex)-ZSM-5, (c) H-M, and (d) H-Y.

Table 2. Aluminum Content of the Zeolites Calculated from ^{27}Al MAS NMR Spectra and the Yields of $DPHT^{+\bullet}$ and $HDPHT^{+}$[a]

sample	Si/Al	Al_f	Al_{nf}	Al_{nf}/Al_f	$DPHT^{+\bullet}$	$HDPHT^{+}$
H,Na-ZSM-5	25	3.0	0.7	0.23	0.43	0.40
Na(ex)-ZSM-5	26	3.0	0.6	0.20	0.37	0.18
H-M	9.0	3.6	1.2	0.33	0.33	0.33
H-Y	2.95	30.4	18.2	0.59	0.11	0.35
UHY[b]	2.8	36.5	19.2	0.53	0.37	0.36

[a] Al_f and Al_{nf} are the number of framework and nonframework Al atoms per unit cell, respectively. The number of $DPHT^{+\bullet}$ radical cations is $1 - R_t$, where R_t is the ratio of the intensity of diffuse light reflected from the sample containing the observed species to the intensity when the observed species is absent. [b] Data taken from ref 22.

tions produce a large and small amount of nonframework Al, respectively.[15] Still, some dealumination of NH_4^+-zeolites upon calcination is unavoidable, irrespective of the conditions.[21] The ^{27}Al MAS NMR spectra of NH_4^+-zeolites calcined at 550 °C (see Figure 1) show two groups of lines at ca. 50 and 0 ppm corresponding respectively to 4-fold coordinated framework Al (50 ppm) and 6-fold coordinated nonframework Al (0 ppm).[19,20] The presence of 6-fold coordinated Al species thus demonstrates that dealumination has taken place. The amounts of both kinds of Al can be calculated using the ^{27}Al spectra and the chemical compositions of the samples (see Table 2).

Calcination of zeolite TPA,Na-ZSM-5 (Si/Al = 25) leads to the decomposition of the TPA^+ cation and gives H,Na-ZSM-5.

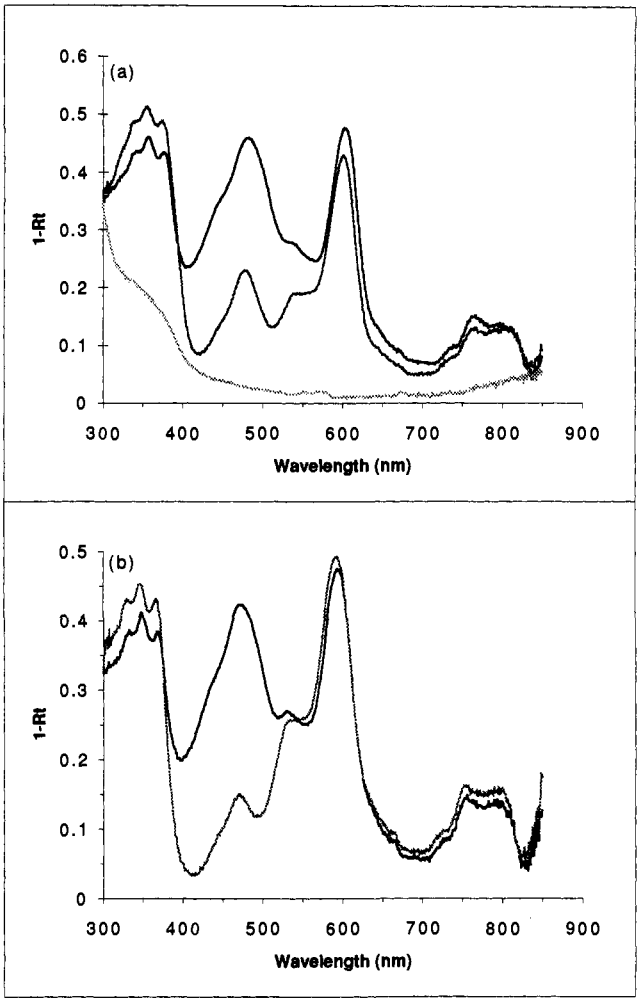

Figure 2. (a) Diffuse reflectance spectra of DPHT adsorbed in Na-ZSM-5 (dotted line), H,Na-ZSM-5 (solid line), and Na(ex)-ZSM-5 (dashed line). (b) Changes of diffuse reflectance spectra of DPHT adsorbed in H,Na-ZSM-5 before (solid line) and after (dashed line) exposure to air. R_t is the ratio of the intensity of diffuse light reflected from the sample containing the observed species to the intensity when the observed species is absent.

In view of the dealumination, the product contains 0.7 nonframework Al atoms per unit cell (Al/u.c.) (19% of the total Al content) which give the ^{27}Al line at 0.8 ppm (see Figure 1). 2-Fold ion exchange with a 0.2 M aqueous solution of NaCl at room temperature removes some of the nonframework Al, but 0.6 Al/u.c. (now at 1.8 ppm) still remain in sample Na(ex)-ZSM-5 (Table 2), so that the process is insufficient for a complete removal of the nonframework Al from ZSM-5. Calcination of NH_4-M (Si/Al = 9.0) creates 1.2 nonframework Al/u.c. (25% of the total Al content) resonating at 1.8 ppm.

^{27}Al MAS NMR shows that zeolite H-Y (Si/Al = 2.95) contains 37% (18.2 nonframework Al/u.c.). Calcination of zeolite NH_4-Y (Si/Al = 2.95) under "deep bed" conditions creates more nonframework aluminium and ultrastablilizes the zeolite. By comparing the Si/Al ratio from chemical analysis with that calculated from the ^{29}Si MAS NMR spectrum,[22] we see that 19.2 nonframework Al/u.c. remain[22] (Table 2). ^{27}Al MAS NMR detects no extraframework Al in zeolites Na-Y, Na-M, and Na-ZSM-5 calcined under the same conditions.

(21) Maesen, T. L. M.; Sulikowski, D.; van Bekkrm, H.; Kouwenhoven, H. W.; Klinowski, J. *Appl. Catal.* **1989,** *48,* 373.

(22) Liu, X.; Klinowski, J.; Thomas, J. M. *J. Chem. Soc., Chem. Commun.* **1986,** 582.

Scheme 2. Protonated Species Formed from the Probe Molecules

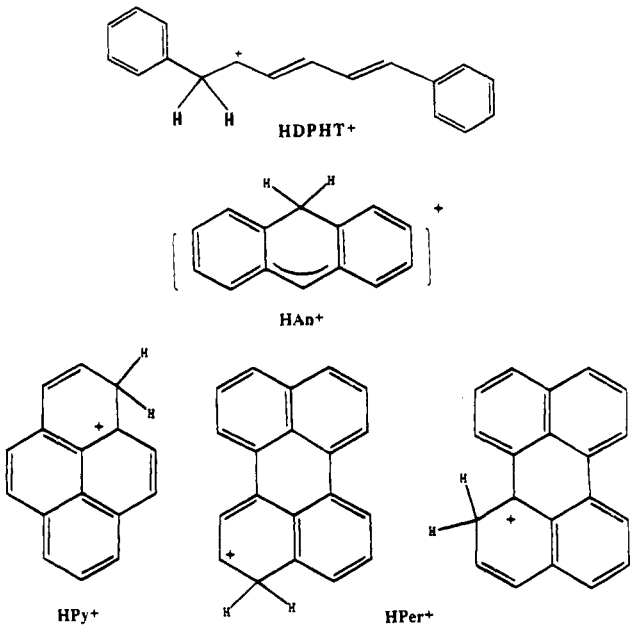

DPHT in ZSM-5, Mordenite, and Y

Given the narrowness of the channels of ZSM-5, only the DPHT molecule was studied for this sample. Figure 2a gives the steady-state diffuse reflectance spectra of DPHT adsorbed in Na-ZSM-5 (6.1×10^{-6} mol of DPHT/g), H,Na-ZSM-5 (9.9×10^{-6} mol/g), and Na(ex)-ZSM-5 (1.0×10^{-5} mol/g). We see that the amount of DPHT adsorbed in Na-ZSM-5 is lower than in the other two samples, which is in agreement with the results of the analysis of the supernatant solutions. The low sorption capacity of Na-ZSM-5 is the consequence of the channels being blocked by the Na^+ cations. The absorption band at ca. 350 nm is structureless, while the other two samples give structured bands. The structureless absorption band from DPHT is in agreement with this interpretation and is brought about by the "tight fit" of the molecule to the channel wall. H,Na-ZSM-5 adsorbs 1.6 times as many DPHT molecules as Na-ZSM-5 and gives a spectrum with bands at 346, 360, 380, 440 (shoulder), 480, 540, 605, 764, and 811 nm (Figure 2a). The bands at 346, 360, and 380 nm are due to neutral DPHT molecules and those at 540, 605, 764, and 811 nm to $DPHT^{+\bullet}$ cation radicals (in agreement with the results of Ramamurthy et al.[10]). The band at 480 nm, which was not observed earlier,[10] is not sensitive to exposure of the sample to 600 Torr of O_2 overnight. However, upon exposure to laboratory air, the intensity of the new band decreases rapidly, which is accompanied by an increase of the intensity of the band from DPHT (see Figure 2b) and a color change of the sample from green to blue. The intensity of the $DPHT^{+\bullet}$ band does not have significant change during this process. We conclude that moisture causes the decay of the species responsible for the 480 nm band and that a direct link exists between this species and neutral molecules, rather than cation radicals. We assign the new band to $HDPHT^+$, i.e. protonated DPHT (Scheme 2). The structure of the protonated DPHT given in Scheme 2 is based on results of theoretical calculations of the charge on each carbon of the molecule using the SPARTAN program.[23] The results from the program (using both AM1 and PM3)[23] clearly indicate that the double-bond carbon is the one to be attacked by a proton. This is consistent with the fact that protonation of double-bond molecules is easier than that of their corresponding aromatic molecules.[24] Further calculations of the protonated species with different configurations which the proton attacks on different carbons of the double bonds or the aromatic rings show that the species given in Scheme 2 is the most stable one. Studies of other organic molecules (see below) also support the protonation.

Adsorption of DPHT on Na(ex)-ZSM-5 produces the same species as those in H,Na-ZSM-5 but in different relative amounts. The concentration of DPHT in Na(ex)-ZSM-5 is higher, while those of $DPHT^{+\bullet}$ and $HDPHT^+$ are 11% and 54% lower, respectively (Figure 2a). ^{27}Al MAS NMR shows that ion exchange removes not only H^+ but also the nonframework Al species. We therefore attribute the large decrease of the yield of $HDPHT^+$ to the removal of H^+ and the slight decrease of the yield of $DPHT^{+\bullet}$ to the removal of 14% of nonframework Al species. The formation of $HDPHT^+$ is thus directly related to the acidic hydroxyl groups, and the formation of $DPHT^{+\bullet}$, to the interaction of DPHT with nonframework Al species. Table 3 summaries the diffuse reflectance spectra and assigns the various bands.

After the DPHT solution is added to the zeolite/*n*-pentane slurry, Na-M turns bluish and H-M green. Figure 3a shows the diffuse reflectance spectra of DPHT-Na-M and DPHT-H-M immediately after adding DPHT. Absorption bands of DPHT in DPHT-Na-M are in the region of 300–400 nm, and weak absorptions from $DPHT^{+\bullet}$, at ca. 620 and 800 nm. The $HDPHT^+$

Table 3. Assignment of Absorption Bands of the Species Observed in Zeolites

zeolite	absorption bands (nm)	assignment
DPHT-Na-ZSM-5	350 (broad)	DPHT
DPHT-H,Na-ZSM-5	346, 360, 380	DPHT
	440 (sh), 480	$HDPHT^+$
	540, 605, 764, 811	$DPHT^{+\bullet}$
DPHT-Na(ex)-ZSM-5	346, 360, 380	DPHT
	440 (sh), 480	$HDPHT^+$
	540, 605, 764, 811	$DPHT^{+\bullet}$
DPHT-Na-M	300–400	DPHT
	620, 800	$DPHT^{+\bullet}$
DPHT-H-M	330	DPHT
	540, 610, 760, 820	$DPHT^{+\bullet}$
	395, 482	$HDPHT^+$
An-H-M	314, 333, 343, 354, 525, 559, 571, 608, 623, 656, 719, 829	$An^{+\bullet}$
	422	HAn^+
Py-H-M	335, 364	Py
	475	HPy^+
	450	$Py^{+\bullet}$
DPHT-Na-Y	355, 371	DPHT
DPHT-H-Y	394	DPHT
	492	$HDPHT^+$
	574, 623	$DPHT^{+\bullet}$
DPHT-UHY	355, 371	DPHT
	487	$HDPHT^+$
	562, 623	$DPHT^{+\bullet}$
An-H-Y	316, 336, 344, 355, 524, 557, 571, 608, 625, 662, 722	$An^{+\bullet}$
	422	HAn^+
Py-H-Y	336, 365	Py
	450–520	HPy^+
	380, 502, 513, 450, 479, 572, 662, 793	$Py^{+\bullet}$
Per-H-Y	336, 392, 464 (sh), 544, 706, 735	$Per^{+\bullet}$
	392, 411, 441, 629	$HPer^+$

(23) Hehre, W. J.; Burke, L. D.; Shusterman, A. J. *SPARTAN, Version 3.0*, Wavefunction, Inc., 1993.

(24) Deno, N. C.; Pittman, C. U. *J. Am. Chem Soc.* **1964**, *87*, 1871.

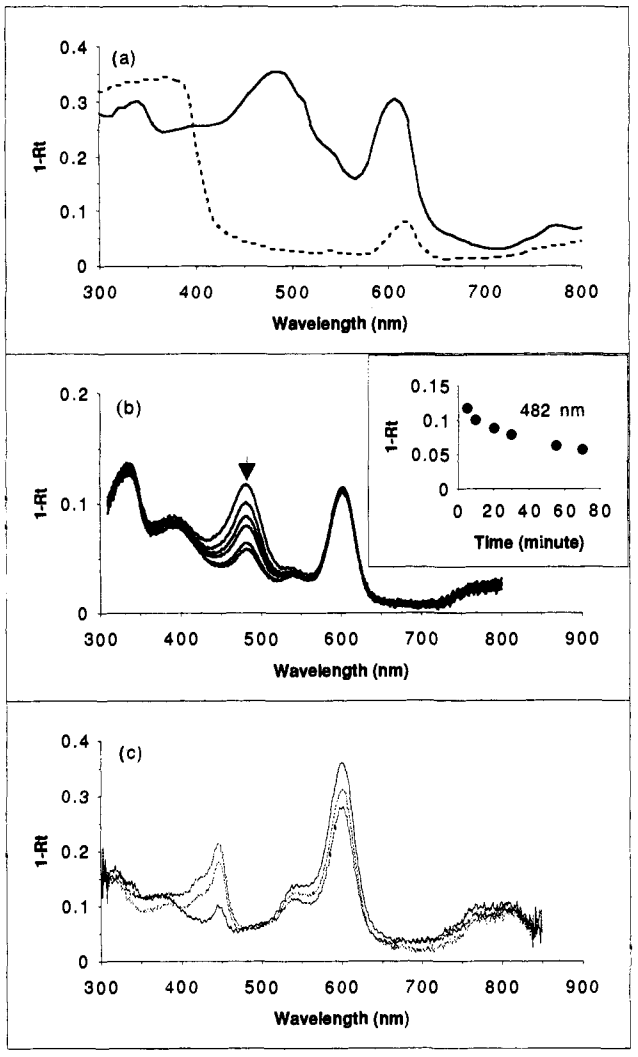

Figure 3. (a) Diffuse reflectance spectra of DPHT in zeolites Na-M (dashed line) and H-M (solid line) immediately after adding the solution of DPHT in *n*-pentane. (b) Change in the diffuse reflectance spectra of DPHT adsorbed in zeolite H-M with time. The insert shows the decay of $HDPHT^+$ (the 482 nm band). (c) Change in the diffuse reflectance spectra of DPHT-H-M immediately after evacuation (solid line), after 1 day (dashed line), and after 5 days (dotted line).

bands (at 480 nm) found in H,Na-ZSM-5 are absent because of the absence of H^+, which confirms that Brønsted acid sites are instrumental in generating $HDPHT^+$. $DPHT^{+\bullet}$ absorption bands are found in Na-M probably because of the presence of a trace amount of nonframework Al species, too small to be detected by ^{27}Al NMR.

In contrast to DPHT-Na-M, the spectrum of DPHT-H-M now contains not only DPHT (at ca. 330 nm) and $DPHT^{+\bullet}$ bands (at 540, 610, and 760 nm) but also the broad band at 482 nm from $HDPHT^+$ (see Figure 3a) due to the presence of H^+ and nonframework Al (1.2 Al/u.c.). The intensities of bands from $DPHT^{+\bullet}$ are significantly enhanced owing to the presence of a large amount of nonframework Al (1.2 Al/u.c.) in the HM sample. Figure 3b shows the changes of the spectra of DPHT-H-M as a function of time. In contrast to $DPHT^{+\bullet}$, $HDPHT^+$ is unstable and its concentration gradually decreases. The decrease of $HDPHT^+$ in H-M is much faster than in H,Na-ZSM-5 and begins when the zeolite is still in the slurry.

Exposure of the sample to air accelerates the decay of $HDPHT^+$ and brings about a color change from green to blue. Within the 2 min needed for filtering and transferring the sample,

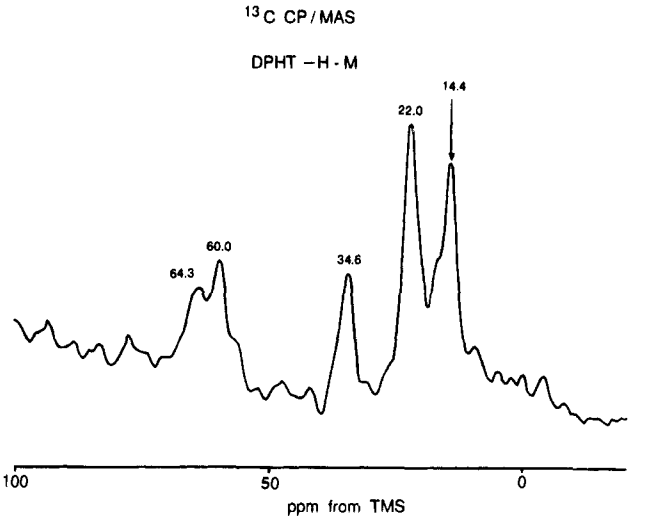

Figure 4. ^{13}C CP/MAS NMR spectrum of DPHT-H-M.

Scheme 3. Oxygenation of $DPHT^{+\bullet}$ Cation Radicals via Reactions with Atmospheric O_2

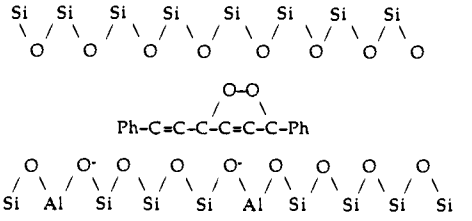

the bands of $HDPHT^+$ disappear completely and those of $DPHT^{+\bullet}$ become dominant (see Figure 3c). Later, two new bands at 430 and 450 nm appear and gradually increase at the expense of $DPHT^{+\bullet}$. This suggests that a new species, not observed in ZSM-5, is produced from a further reaction of $DPHT^{+\bullet}$ cation radicals. The accumulation of this species is slower than the rate of conversion of $HDPHT^+$ to the neutral molecule and may take days to complete. Figure 3c shows the spectral changes after 1 and 5 days.

In order to elucidate the nature of the new species, we have studied DPHT-H-M by ^{13}C CP/MAS NMR (see Figure 4). The chemical shifts of the five peaks (14.4, 22.0, 34.6, 60.0, and 64.3 ppm) show that the residual *n*-pentane molecules (lines at 14.4, 22.0, and 34.6 ppm) are present in the zeolitic channels.[25] This indicates that the blocking of the channels by DPHT results in the occlusion of solvent molecules. The new species found by UV–vis reflectance (Figure 3c) gives NMR lines at 60.0 and 64.3 ppm. Unfortunately, ^{13}C CP/MAS does not reveal lines from carbons in aromatic rings and the double bonds of DPHT, expected at ca. 100–130 ppm. This may be due to very long T_{1r} for ^{1}H. The chemical shifts of the lines at 60.0 and 64.3 ppm suggest that $DPHT^{+\bullet}$ cation radicals are oxygenated via reactions with atmospheric O_2. We believe that the product is that shown in Scheme 3. Other forms of oxygenated species may also be possible such as perepoxide. Its formation requires a sufficient space in zeolite channels for O_2 to diffuse in. The channels of zeolites H-M and H-Y fulfil this requirement. However, $DPHT^{+\bullet}$ molecules fit too tightly into the narrower channels of ZSM-5 to be able to create space for O_2.

Figure 5a shows diffuse reflectance spectra of DPHT-Na-Y, DPHT-HY, and DPHT-UHY. A single absorption in the 300–400 nm region indicates that only the DPHT molecules are present in Na-Y. We attribute the bands at 394, 492, and 623

(25) *The Sadtler Guide to Carbon-13 NMR Spectra.* Simons, W. W., Ed; Sadtler: U.S.A., 1983.

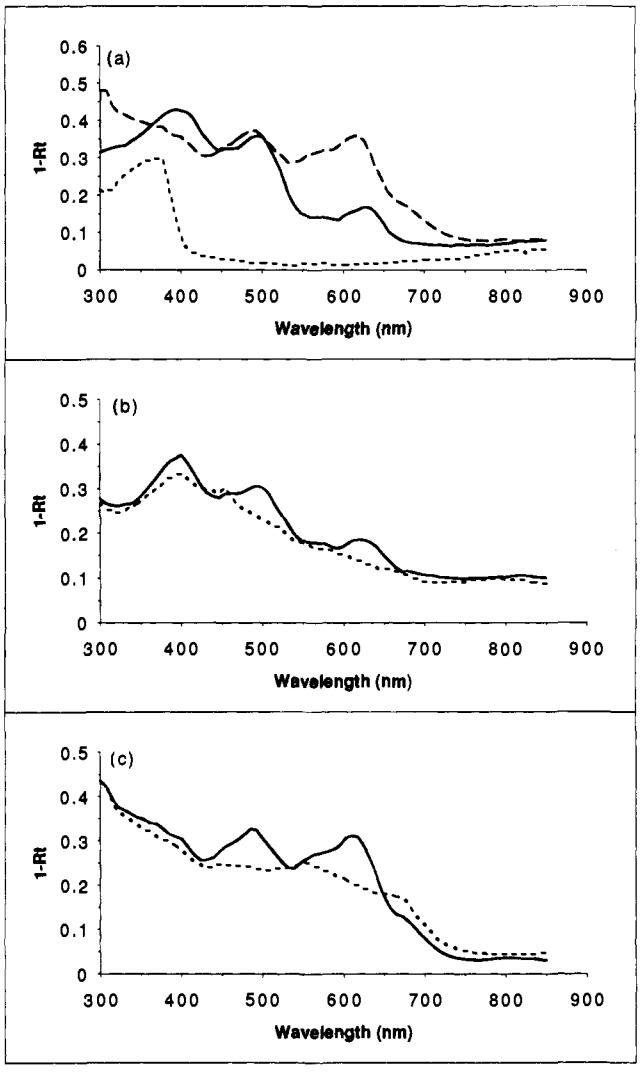

Figure 5. (a) Diffuse reflectance spectra of DPHT-Na-Y (dotted line), DPHT-H-Y (solid line), and DPHT-UHY (dashed line) in *n*-pentane. (b) Diffuse reflectance spectra of DPHT-H-Y before (solid line) and after (dashed line) filtration of *n*-pentane. (c) Diffuse reflectance spectra of DPHT-UHY immediately after preparation (solid line) and after 3 days (dashed line).

nm in H-Y to DPHT, $HDPHT^+$, and $DPHT^{+\bullet}$, respectively. The $DPHT^{+\bullet}$ band in UHY is much stronger than in DPHT-H-Y, indicating that more $DPHT^{+\bullet}$ is produced.

Removal of the solvent from DPHT-H-Y changes the spectrum as shown in Figure 5b, while the spectrum of DPHT-UHY is unaffected. This implies that the molecules of DPHT in UHY are "protected". The spectrum of DPHT-H-Y covers almost the entire spectral range of 400−700 nm, with a band at 450 nm superimposed. The latter band comes from the product of further reactions of $DPHT^{+\bullet}$, as already observed in DPHT-H-M. The broad absorption from DPHT-H-Y is probably due to the different configurations of the adsorbed DPHT molecules. The species found in zeolites H-Y and UHY are unstable and evolve as seen in Figure 5c.

Anthracene, Pyrene, and Perylene in Mordenite and Y

Adsorption of anthracene on H-M and HY causes immediate color changes of the samples from white to green. Figure 6 shows the diffuse reflectance spectra of An-H-M at different time intervals. The absorption bands for these two samples are listed in Table 3. From the literature reports,[26-30] it is known that the $An^{+\bullet}$ cation radical (see the bands in Table 3) and

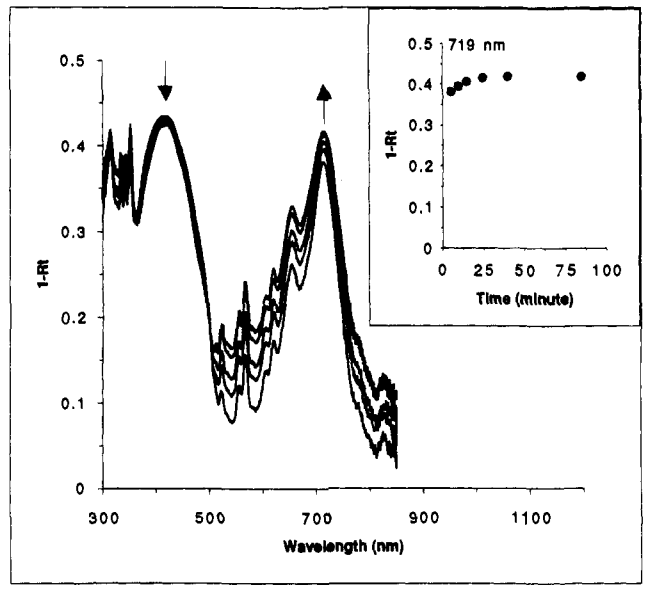

Figure 6. Diffuse reflectance spectra of An-H-M at different times after adding An. The insert is the plot of the yield change of $An^{+\bullet}$ as a function of time.

protonated anthracene, HAn^+ (broad band around 422 nm), are created in these samples (see Scheme 2). Absorption bands of An are in the 300−400 nm region and overlap with the broad band from HAn^+. As seen from the instantaneous color change, HAn^+ and $An^{+\bullet}$ form immediately after the addition of An. The spectrum evolves slowly with time: the amount of $An^{+\bullet}$ increases, and that of neutral molecules decreases (see Figure 6).

Adsorption of pyrene on H-M and H-Y changes the color of the samples from white to yellow-green. Diffuse reflectance spectra of Py-H-Y given in Figure 7a show the presence of Py, $Py^{+\bullet}$, and HPy^+ (see Scheme 2), with absorption bands at ca. 300−370 nm, ca. 380−800, and at ca. 450−520 nm, respectively (Table 3).[26] Because the bands of $Py^{+\bullet}$ and of HPy^+ overlap, a difference spectrum is given to reveal the bands of the latter (Figure 7b). The intensity of the HPy^+ band, with a maximum at 513 nm, gradually increases, and that from Py decreases (note the negative bands in Figure 7b), indicating that HPy^+ is formed at the expense of Py. By contrast, the bands of $Py^{+\bullet}$ are unchanged. The insert in Figure 7a gives the intensity changes of HPy^+. The formation of HPy^+ in H-Y is much slower than that of $An^{+\bullet}$, and maximum yield is reached within 80 min.

Because of the light sensitivity of perylene, Per-H-Y was prepared in the dark. Figure 8 gives the diffuse reflectance spectra, and Table 3 lists the absorption bands. As with Py-H-Y, the $Per^{+\bullet}$ cation radical[26] is formed together with another species absorbing at ca. 629 nm. This is assigned to $HPer^+$ in Scheme 2,[26-30] which gives two spectroscopically indistinguish-

(26) Shida, T. *Electronic Absorption Spectra of Radical Ions;* Physical Science Data 34, Elsevier: Amsterdam, 1988.
(27) Aalbersberg, W. I.; Hoijtink, G. J.; Mackor, E. L.; Weijland, W. P. *J. Chem. Phys.* **1959,** 3049.
(28) Dallinga, G.; Mackor, E. L.; Verrijn Stuart, A. A. *Mol. Phys.* **1958,** *1,* 123.
(29) (a) Gold, V.; Tye, F. L. *J. Chem. Soc.* **1952,** 2173. (b) Gold, V.; Tye, F. L. *J. Chem. Soc.* **1952,** 2181. (c) Gold, V.; Tye, F. L. *J. Chem. Soc.* **1952,** 2184.
(30) (a) Olah, G. A.; Pittman, C. U. Jr.; Symons, M. C. R. *Carbonium Ions. General Aspects and Methods of Investigation*; Olah, G. A.; Schleyer, P. v. R., Eds.; Interscience Publishers: New York, 1968; Vol. 1, p 153. (b) Brouwer, D. M.; Mackor, E. L.; Maclean, C. *Carbonium Ions. Methods of Formation and Major Types*; Olah, G. A.; Schleyer, P. v. R., Eds.; Interscience Publishers: New York, 1970; Vol. II, p 837.

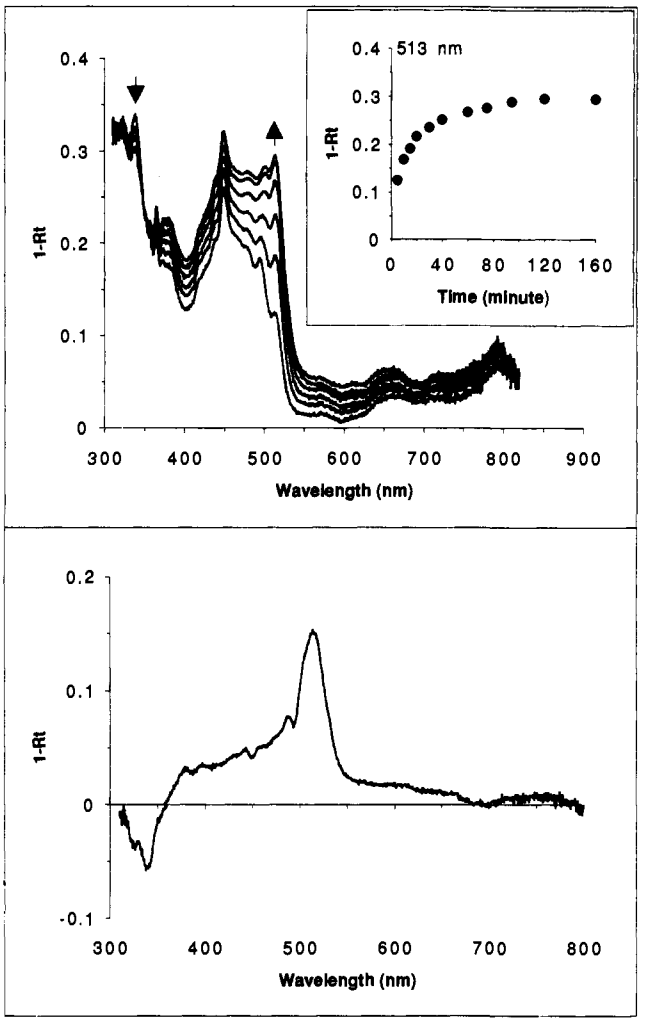

Figure 7. (top) Changes in the diffuse reflectance spectra of Py-H-Y with time. The insert plots the relative intensity of HPy^+ monitored at 513 nm. (bottom) Difference between the first and the last spectrum in a.

able configurations for $HPer^+$.[29,30] The amount of the species absorbing at 629 nm does not change, while that of $Per^{+\bullet}$ increases and that of Per decreases. Absorption bands from Per overlap with those of $HPer^+$ (see the 350−450 nm region in Figure 8). The insert shows the intensity change of $Per^{+\bullet}$. The change is faster than that of $Py^{+\bullet}$ but slower than that of $An^{+\bullet}$ (compare Figures 6, 7a, and 8).

Emission of the Protonated Species

Further evidence for the presence of protonated species in H^+-zeolites comes from fluorescence studies. Figure 9 shows typical steady-state emission spectra of $HDPHT^+$, HAn^+, HPy^+, and $HPer^+$. A broad structureless band is observed for each with a maximum at 540 nm for $HDPHT^+$, 545 nm for HAn^+, 535 nm for HPy^+, and at 660 nm for $HPer^+$. Similar emission was also observed for HPy^+ in strong acid $HClO_4$, indicating that the species in zeolites and in acid solution are the same. The emission spectra observed are mirror images of their corresponding absorption spectra, confirming the origin of the emission. The Stoke's shifts are ~60 nm for $HDPHT^+$, ~120 nm for HAn^+, ~25 nm for HPy^+, and ~30 nm for $HPer^+$. Lifetime measurements give 1.1−1.7 ns and 3.8−3.9 ns for HAn^+ and HPy^+ in H-M and H-Y, respectively, so that the excited protonated species are short-lived. The short emission lifetime of the excited protonated species depends on their nature

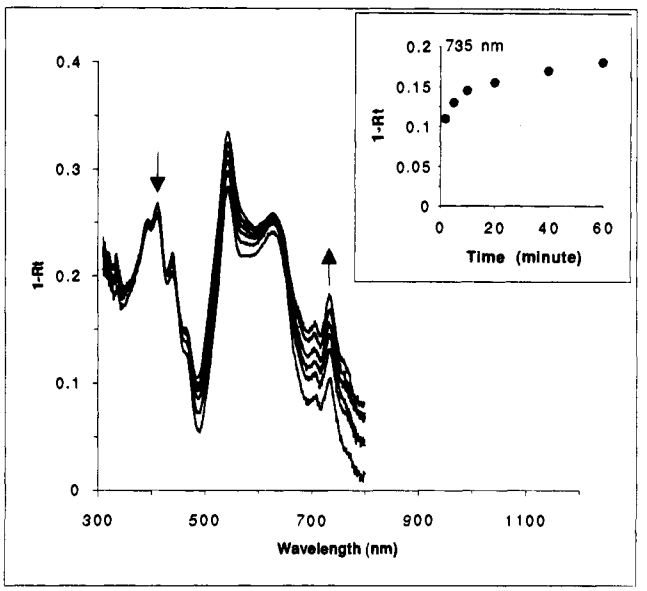

Figure 8. Changes in the diffuse reflectance spectra of Per-H-Y with time. The insert plots the change of the relative intensity of $Per^{+\bullet}$ monitored at 735 nm.

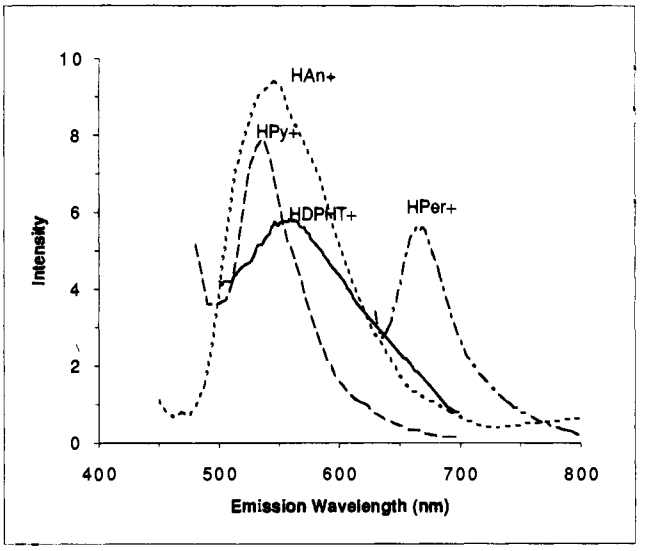

Figure 9. Typical steady-state emission spectra of $HDPHT^+$, HAn^+, HPy^+, and $HPer^+$ in zeolites.

and may also be shortened by the presence of cation radicals as a result of the overlap of their emission bands with the absorption bands of the cation radicals (energy transfer).

Emission from cation radicals in zeolites is expected in the region >850 nm. The emission of $DPHT^{+\bullet}$ in ZSM-5 has indeed been observed at ca. 880 and 1000 nm,[10] that of $Per^{+\bullet}$ on the surfaces of laponite[31] and γ-alumina[32] at ca. 810 and 925 nm, and that of $Py^{+\bullet}$ on the surface of laponite at 825 nm.[31]

Discussion

High-temperature calcination of NH_4^+-zeolites produces their strongly acidic H^+-forms. ^{27}Al NMR shows that nonframework aluminum, associated with Lewis acidity, is generated at the same time irrespective of the conditions of calcination.[21] Interactions between adsorbed basic molecules and the acid sites

(31) In, K.-K.; Liu, X.; Thomas, J. K. *Chem. Phys. Lett.* **1991,** *186,* 198.
(32) Pankasam, S.; Iu, K.-K.; Thomas, J. K. *J. Photochem. Photobiol., A* **1991,** *62,* 53.

lead to protonated species and cation radicals. In solutions of strong acids, the formations of protonated species of aromatic molecules are well established[27-30] and their electronic spectra were extensively studied.[27-30] The formation of cation radicals of aromatic molecules depends on whether oxidizing agents, such as O_2 or SO_3, are present.[27,28] Without these, only the protonated species form; in the presence of oxidizing agents, protonated species are converted to cation radicals.[27,28] However, in zeolites, protonated species and cation radicals are concurrently produced. Both are independently related to the corresponding neutral molecules. There is no interconversion between the two kinds of species.

Protonation of organic molecules in H^+-zeolites has been proposed on the basis of sorption studies[33] and the mechanisms of catalytic reactions of hydrocarbons.[34] Our UV–vis spectroscopic studies provide direct evidence for such protonation. Protonated species formed in H^+-zeolites are unstable and convert back to neutral molecules in the presence of water. The loss of H^+ by $HDPHT^+$ is more rapid than for other arenes, which highlights the difference between molecules containing double bonds and aromatic rings. Because of their unstability, the protonated species may be very difficult to observe, as happened to Ramamurthy et al., who exposed their samples to atmospheric air during sample transfer.[10]

The stabilities of protonated species and cation radicals are affected not only by the nature of the molecules but also by the size of the cavities and channels. The accumulation curves of cation radicals and protonated species reflect diffusion in the intracrystalline space. In large-pore zeolites with small adsorbed molecules (see Table 1 and Scheme 1), diffusion is fast: cation radicals and protonated species accumulate quickly. The reverse is true for narrow-channel zeolites with large adsorbed molecules. The rates of accumulation of An, Py, and Per in H-Y (see Figures 6, 7a, and 8) follow the sequence An > Per > Py, which seems to disagree with the sizes of Py and Per given in Table 1. However, because the Per molecule is not planar, the molecule may find it easier to diffuse through the windows of the supercage than the planar Py molecule.

If a molecule fits tightly into the cavities or channels, it is "protected" by the framework and no further changes of the species can be observed. DPHT-ZSM-5 is an example of this situation. As a result of the tight fit of DPHT, no further changes could be observed for the $DPHT^{+\bullet}$ produced. This was also observed by Ramamurthy et al.,[10] and no changes of $DPHT^{+\bullet}$ radical were seen even upon boiling the sample in methanol or water.[10] In contrast to ZSM-5, $DPHT^{+\bullet}$ in H-M, where the channels are slightly wider, undergoes further reactions (see Figure 3c). In large-pore zeolites, such as H-Y and UHY, the changes of $DPHT^{+\bullet}$ are more rapid still (see Figure 5).

The role of nonframework Al in the formation of cation radicals is evident from the comparison of results from the same zeolite but with different amounts of nonframework Al. For example, H,Na-ZSM-5 and Na(ex)-ZSM-5 give different yields of cation radicals corresponding to the different amounts of the nonframework Al. Table 2 summaries the data on DPHT. However, a correlation between the different types of samples cannot be made because of the differences in structure and the degree of confinement of the molecules. On the other hand, in "cage" (as opposed to "channel") zeolites, the location of nonframework Al could be another factor which complicates any correlation.

In view of the concurrent formation of protonated species and cation radicals, the adsorbed molecules play a dual role in response to protonation and electron donation. The strengths and distributions of the Brønsted and Lewis acid sites must be a key factor in determining which reaction takes place. Proton affinity (PA) and ionization potential (IP) of the molecules must be another key factor. Because the proton–acceptor and electron–donor abilities of the molecules under study follow the same sequence; i.e. Py (PA = 206.1 kcal/mol; IP = 7.5 eV) > An (PA = 207.0 kcal/mol; IP = 7.0 eV) > Per (PA = 211.4 kcal/mol; IP = 6.5 eV),[35,36] the type of reaction which occurs for the same adsorbed compound is determined solely by the zeolite. This is demonstrated by the different behaviors of Py, An, and Per in zeolite H-Y. For molecules with IP < 7.0 eV and PA > 207 kcal/mol, an increased yield of cation radicals is observed, while for molecules with IP > 7.0 eV and PA < 207 kcal/mol, there is an increased yield of protonated species. The same is true for Py and An in zeolite H-M. However, the simultaneous presence of protonated species and cation radicals in these zeolites suggests that strong Brønsted and Lewis acid sites are always present.

Weak acidic sites are also found in H^+-zeolites, as seen from the presence of neutral molecules. However, a close look at the spectra of these reveals that neutral molecules do not have exactly the same configuration as in solution and that band broadening and spectral shift are evident. A comparison of the spectra of DPHT in H^+-zeolites with different structures clearly shows these characteristics: well-resolved bands in H-ZSM-5 (Figure 2), one broad band at 330 nm in H-M (Figure 3), and a broad band at 394 nm in H-Y (Figure 5). These differences demonstrate that the nature of the adsorbed molecules is intermediate between those of the cation radical, protonated species, and neutral molecule. If this is taken into consideration, the neutral molecules assigned in Table 3 may be better described as charge-transfer complexes.

Acknowledgment. We are grateful to the U.S. National Science Foundation for support, Dr. Shikai Zhao for help with the Macromodel program, and Dr. Ziqi Jiang for discussions.

(33) Naccache, C.; Chen, F. R.; Coudurier, G. In *Zeolites: Facts, Figures, Future;* Jacobs, P. A.; van Santen, R. A., Eds.; Elsevier: Amsterdam, 1989; p 66.

(34) Poutsma, M. L. In *Zeolite Chemistry and Catalysis;* Rabo, J. A., Ed.; ACS Monograph 171, American Chemical Society: Washington, DC., 1976; p 437.

(35) Birks, J. B. *Photophysics of Aromatic Molecules;* Wiley-Interscience: New York, 1970; p 457.

(36) Lias, S. G.; Liebman, J. F.; Levin, R. D. *J. Phys. Chem. Ref. Data* **1984,** *13,* 695.